JACS
JOURNAL OF THE AMERICAN CHEMICAL SOCIETY
Article
pubs.acs.org/JACS

Ligand Exchange-Mediated Activation and Stabilization of a Re-Based Olefin Metathesis Catalyst by Chlorinated Alumina

Alessandro Gallo,[†] Anthony Fong,[†] Kai C. Szeto,[§] Julia Rieb,[‡] Laurent Delevoye,[∥] Régis M. Gauvin,*[,∥] Mostafa Taoufik,*[,§] Baron Peters,*[,†,‡] and Susannah L. Scott*[,†,‡]

[†]Department of Chemical Engineering and [‡]Department of Chemistry & Biochemistry, University of California, Santa Barbara, California 93106-5080, United States

[§]Laboratoire de Chimie, Catalyse, Polymères et Procédés, UMR 5265 CNRS/ESCPE-Lyon/UCBL, ESCPE Lyon, F-308-43, Boulevard du 11 Novembre 1918, F-69616 Villeurbanne Cedex, France

[∥]Univ. Lille, CNRS, Centrale Lille, ENSCL, Univ. Artois, UMR 8181, UCCS - Unité de Catalyse et Chimie du Solide, F-59000 Lille, France

Supporting Information

ABSTRACT: Extensive chlorination of γ-Al_2O_3 results in the formation of highly Lewis acidic surface domains depleted in surface hydroxyl groups. Adsorption of methyltrioxorhenium (MTO) onto these chlorinated domains serves to activate it as a low temperature, heterogeneous olefin metathesis catalyst and confers both high activity *and* high stability. Characterization of the catalyst reveals that the immobilized MTO undergoes partial ligand exchange with the surface, whereby some Re sites acquire a chloride ligand from the modified alumina while donating an oxo ligand to the support. More specifically, Re L_{III}-edge EXAFS and DFT calculations support facile ligand exchange between MTO and Cl−Al_2O_3 to generate [$CH_3ReO_2Cl^+$] fragments that interact with a bridging oxygen of the support via a Lewis acid−base interaction. According to IR and solid-state NMR, the methyl group remains intact, and does not evolve spontaneously to a stable methylene tautomer. Nevertheless, the chloride-promoted metathesis catalyst is far more active and productive than MTO/γ-Al_2O_3, easily achieving a TON of 100 000 for propene metathesis in a flow reactor at 10 °C (compared to TON < 5000 for the nonchlorinated catalyst). Increased activity is a consequence of both a larger fraction of active sites and a higher intrinsic activity for the new sites. Increased stability is tentatively attributed to a stronger interaction between MTO and chlorinated surface regions, as well as extensive depletion of the Brønsted acidic surface hydroxyl population. The reformulated catalyst represents a major advance for Re-based metathesis catalysts, whose widespread use has thus far been severely hampered by their instability.

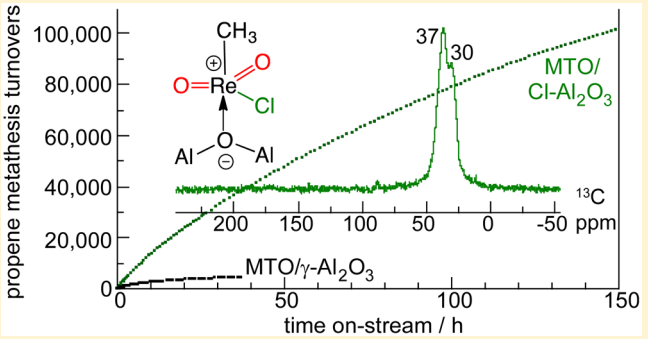

INTRODUCTION

Olefin metathesis is practiced on a large-scale in Shell's Higher Olefins Process (SHOP), Phillips' neohexene process, and ABB Lummus' Olefins Conversion Technology (OCT).[1] The supported Mo and W oxides used as catalysts in these gas-phase applications require elevated operating temperatures. For example, the SHOP metathesis catalyst (MoO_3/γ-Al_2O_3) operates at 100−200 °C, while the WO_3/SiO_2 catalyst used for OCT and the neohexene process requires at least 400 °C.[2,3] Re_2O_7 is the only oxide that, when dispersed on a suitable support, shows metathesis activity below 100 °C, making it better suited for liquid-phase metathesis involving heavier olefins. It is used in producing α,ω-diolefins such as 1,5-hexadiene and 1,9-decadiene by ethenolysis of cycloolefins in Shell's FEAST (Further Exploitation of Advanced Shell Technology) process,[4] as well as in Axens' Meta-4 Process for the production of propene from ethene and 2-butenes.[5] However, the relatively low activities (TOF < 0.01 s^{-1}) and especially productivities (TON < 100) typical of such catalysts[1] have been major obstacles to their widespread use. Fast deactivation is a particularly severe issue.[6] Commercialization of Re-based catalysts is also hampered by the high cost of Re, the high metal loading required, and the volatility of Re_2O_7 (which results in metal loss during catalyst regeneration by calcination).

The acidity of the catalyst support is a key factor in the activation of dispersed Re oxide precatalysts: various reports have claimed either Brønsted[7,8] or Lewis[9−11] acid sites to be necessary. Since both types of acidity occur together in many oxide supports, the issue has long been controversial. Higher activity was observed upon replacing the typical γ-Al_2O_3

Received: July 5, 2016
Published: August 30, 2016

DOI: 10.1021/jacs.6b06953
J. Am. Chem. Soc. 2016, 138, 12935−12947

support by organized mesoporous alumina (OMA) with greater Lewis acidity[10,12,13] (although this claim has been challenged).[14] Catalysts based on supported methyltrioxorhenium (MTO) have been proposed as more active alternatives to supported ReO_x catalysts,[15] facilitated by the development of efficient methods for MTO synthesis.[16−18] MTO can also be generated (or regenerated) in situ from inorganic perrhenates by treatment with a methylating agent, such as $SnMe_4$ or $AlMe_3$.[19] In solution, MTO requires activation by a Lewis acid[20] such as $AlCl_3$ (in combination with $SnMe_4$) or $AlCl_xMe_y$.[21] However, deposition of MTO on an acidic oxide such as SiO_2−Al_2O_3,[19,22−26] niobia,[23,27,28] zeolite Y,[29] γ-Al_2O_3,[23,30] or OMA[26,31,32] is even more effective. Interaction with purely Brønsted acidic supports such as K10-montmorillonite or sulfated Al_2O_3 does not yield an active catalyst.[33] While strong Brønsted acid sites appear to be ineffective in activating MTO,[33] their presence has been implicated in decreased selectivity and deactivation.[25] MTO is completely inactive for metathesis in the presence of weakly acidic SiO_2.[24,33]

Unlike conventional Re_2O_7/γ-Al_2O_3 catalysts which develop appreciable metathesis activity only at near-monolayer coverages (typically ≥10 wt % Re), MTO-based catalysts are very active at low Re loadings (<3 wt %).[34] Furthermore, supported MTO-based catalysts (including those in which MTO is formed in situ by reaction of supported perrhenates with $SnMe_4$)[19] are effective as heterogeneous catalysts for the metathesis of olefins bearing polar substituents.[22] For example, MTO-based catalysts catalyze the selective metathesis of triacylglycerols from seed oils,[35] in contrast to Grubbs'-type catalysts which favor the formation of insoluble cross-linked polymers.[36,37] Conventional oxide-based heterogeneous catalysts (MoO_3/γ-Al_2O_3, WO_3/SiO_2, and Re_2O_7/γ-Al_2O_3) are inactive toward functionalized olefins.

While MTO is even more active when associated with SiO_2−Al_2O_3 relative to γ-Al_2O_3, the high intrinsic Brønsted acidity of SiO_2−Al_2O_3 promotes undesired side-reactions, including olefin isomerization and oligomerization.[24,33] The metathesis activity of MTO/γ-Al_2O_3 can be enhanced by addition of promoters such as $ZnCl_2$.[26,33,38,39] Initially, both the Lewis acidic metal ion and halide ions were deemed necessary,[33] and they were shown to cause both the fraction of active Re sites, as well as the average per-site activity, to increase.[38]

As the preceding assessment demonstrates, improving heterogeneous catalysts by varying their composition and/or the method of preparation remains a highly empirical activity. Rational design implies a fundamental understanding of the effects of such changes at the molecular level. The transition aluminas, which present a variety of surface OH groups (weak and strong Brønsted acid sites, as well as Brønsted basic sites) and a range of Lewis acid sites, have intrinsically heterogeneous surfaces.[40] Thus, grafted MTO exemplifies a supported organometallic catalyst with highly nonuniform sites, and a very low fraction that are metathesis-active. Even supports with less diverse Al coordination environments, such as high silica-content silica−aluminas, give nonuniform active sites. Thus, MTO supported on SiO_2−Al_2O_3 showed identical activity toward propene regardless of whether the Re loading was 1.0 or 10 wt %.[25] Finally, despite general agreement that terminal carbenes must be present in the active sites, such species have yet to be identified for any supported ReO_x- or MTO-based catalyst. Catalysts prepared by grafting high-valent Re alkylidenes[41] onto oxide surfaces[15,42] are possibly more uniform and therefore easier to characterize, however their exotic ligands and single-use nature make them poorly suited to large-scale, continuous processing of olefins.[2,43,44]

Chlorination of γ-Al_2O_3 and/or the use of chloride-containing Re(V) complexes has been reported to enhance the metathesis activity of supported perrhenate catalysts.[14,45,46] Highly chlorinated aluminas with high Lewis acidity and low Brønsted acidity have long been used as catalyst supports in large-scale hydrocarbon reforming processes.[47] In this study, we grafted MTO directly onto highly chlorinated γ-alumina (Cl−Al_2O_3) in order to explore the effect on the structure of the grafted sites, their activity and stability.

RESULTS AND DISCUSSION

Catalyst Synthesis. Supported MTO catalysts are extremely hygroscopic, and must be assembled and handled without exposure to air. They were prepared by subliming volatile MTO at reduced pressure and room temperature onto a dry, high surface area oxide support. First, γ-Al_2O_3 was calcined in air at 450 °C for 4 h to remove adsorbed hydrocarbons and carbonates, then dried in vacuo (ca. 10^{-4} Torr) at 450 °C. This material has a total surface hydroxyl density of ca. 2.0 OH nm^{-2}.[48−50] Chlorinated alumina was prepared by exposing calcined and dried γ-Al_2O_3 to a stream of CCl_4 at 300 °C prior to a second drying at 450 °C, to produce the material denoted Cl−Al_2O_3. After evacuation at 450 °C, it contains 4.0 wt % Cl, corresponding to a surface density of 3.8 Cl nm^{-2}. Chlorinated and unchlorinated catalysts were prepared by exposing either γ-Al_2O_3 or Cl−Al_2O_3, respectively, to MTO vapor at room temperature. Both materials contain 2.3−2.4 wt % Re.

Effect of Chlorination on Propene Metathesis Activity. Olefin metathesis activity was first assessed in kinetics experiments performed in a batch reactor. Low-pressure, high purity propene was used as the reactant, to facilitate comparison to previously reported rate constants. Using propene/Re = 250, the kinetics of the approach to equilibrium were observed to be pseudo-first-order, Figure 1. For MTO grafted onto γ-Al_2O_3, the apparent second-order rate constant for propene homometathesis was obtained by normalizing k_{obs} by the amount of Re, resulting in k = 540 s^{-1} $(mol_{Re})^{-1}$ at 0 °C (Table 1). For comparison, MTO/SiO_2−Al_2O_3 is ten times more active (k = 5590 s^{-1} $(mol_{Re})^{-1}$) under the same conditions.[25] As we and others have reported,[26,33,38,39] addition of $ZnCl_2$ causes the metathesis activity of supported MTO to increase dramatically, resulting in an activity comparable to that of MTO/SiO_2−Al_2O_3. The second-order rate constant increases with the loading of $ZnCl_2$, Table 1.

Propene homometathesis activity increases even more dramatically when MTO is grafted onto Cl−Al_2O_3. For the conditions shown in Figure 1, the half-life is 0.5 min at 0 °C, compared to more than 17 min for MTO/γ-Al_2O_3 (both containing 2.4 wt % Re). This represents a ca. 30-fold rate enhancement due to chlorination of the support. Furthermore, although the Cl content of the CCl_4-modified Al_2O_3 (4.0 wt %) is comparable to that of a highly $ZnCl_2$-promoted catalyst (Al/Zn = 16, 5.0 wt % Cl), the apparent second-order rate constant is considerably larger, at 18,250 s^{-1} $(mol_{Re})^{-1}$. This finding strongly suggests that *chloride, not* Zn^{2+}*, is principally responsible for the activity enhancement*. Very similar kinetic results were obtained when the reactor was evacuated for an hour and fresh propene was added, confirming the reproducibility of the measurement and the stability of the catalyst (at least over short

DOI: 10.1021/jacs.6b06953
J. Am. Chem. Soc. 2016, 138, 12935−12947

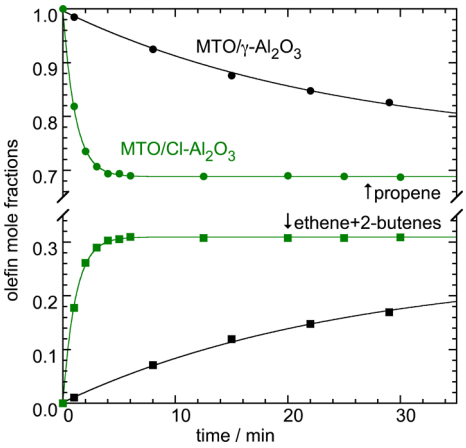

Figure 1. Comparison of kinetic profiles for metathesis of propene (circles) and olefin product formation (ethene+2-butenes, squares), catalyzed by MTO supported on γ-Al_2O_3 (black, 2.4 wt % Re) and on Cl–Al_2O_3 (green, 2.3 wt % Re, 4.0 wt % Cl) in a constant-volume batch reactor. Conditions: 67 mbar propene (C_3/Re = 250), 0 °C, 10 mg catalyst. Solid lines are nonlinear least-squares curve fits of the appropriate form of the integrated first-order rate equation, $n = n_\infty + (1 - n_\infty)e^{-k_{obs}t}$ or $n = n_\infty(1 - e^{-k_{obs}t})$, with two variable fit parameters (n_∞, k_{obs}).

Table 1. Comparison of Apparent Second-Order Rate Constants[a] and Initial Turnover Frequencies[b] for Gas-Phase Propene Homo-Metathesis at 0 °C, by Supported CH_3ReO_3

catalyst	k/s^{-1} (mol$_{Re}$)$^{-1}$	TOF$_{initial}$/ s^{-1}
MTO/γ-Al_2O_3 (2.4 wt % Re)	540[c]	0.20
MTO/SiO_2–Al_2O_3 (1.0 wt % Re)	5590[25]	2.1
MTO/$ZnCl_2$/Al_2O_3 (3.0 wt % Re; Al/Zn = 48)	3350[38]	1.2
MTO/$ZnCl_2$/Al_2O_3 (3.0 wt % Re; Al/Zn = 16)	8380[38]	3.1
MTO/Cl–Al_2O_3 (2.3 wt % Re; 4.0 wt % Cl)	18 250[c]	6.6

[a]For a reversible reaction such as olefin metathesis, the apparent rate constant includes contributions from the forward and reverse rate constants. [b]Calculated from the apparent second-order rate constants, as rates (in mol propene converted per mol Re per s) at t = 0 s (see the Supporting Information). [c]This work. Conditions: constant-volume batch reactor, 67 mbar propene, 0 °C, 10 mg catalyst (2.3–2.4 wt % Re), C_3/Re = 250.

time periods). Ethene and 2-butenes represent 99% of the products (ethene/2-butenes ≈ 1.0) at all times during the reaction; only traces of higher olefins were detected by GC (<1%).

The number of active sites was probed by the active site-counting method of Chauvin and Commereuc.[51] The catalyst was first exposed to 2-butenes (a mixture of *cis* and *trans*) at room temperature to generate ethylidene active sites, followed by several hours of evacuation and exposure to ethene, also at room temperature. The amount of propene liberated in the second step corresponds to the number of active sites present, provided the evacuation period is long enough to remove adsorbed butenes (which could result in significant over-counting). Based on the average of several independent experiments, ca. 2% of Re sites are active on unmodified γ-Al_2O_3, while 12–16% of Re sites are active on Cl–Al_2O_3. Thus, the estimated active site fraction increases 6–8-fold. However, since the overall activity increases ca. 30-fold, we infer that chlorination of γ-Al_2O_3 enhances both the number of active sites *and* the average per-site activity. This in turn implies that at least some of the active sites present on Cl–Al_2O_3 are distinct from those present on γ-Al_2O_3.[52]

Nature of chlorinated γ-Al_2O_3. In order to understand the role of the modified catalyst support in this dramatic rate enhancement, we investigated how chlorination changes the surface properties of γ-Al_2O_3, via its effect on the number and distribution of surface hydroxyls as well as the surface acidity.[53,54] The extent of chlorination is known to depend on the identity of the chlorinating agent and the reaction conditions. Mild chlorination with HCl leads only to replacement of surface OH groups,[55] while use of CCl_4 and more severe reaction conditions causes replacement of lattice oxygen atoms as well,[56] eventually generating volatile $AlCl_3$ by etching of the surface. The high surface density of chloride (3.8 Cl nm^{-2}) in our Cl–Al_2O_3 relative to its initial hydroxyl coverage (ca. 2.0 OH nm^{-2}) implies that chlorination involves not only the replacement of terminal and bridging hydroxyls, but also many bridging oxygens (Al–O–Al), Scheme 1. Although computational modeling reported the presence of bridging chlorides to be unlikely at low Cl loadings and/or high hydroxyl densities,[54] fluorination of alumina was shown to result in incorporation of both terminal and bridging fluorides.[57]

Scheme 1. Possible Reactions Occurring during Extensive Chlorination of γ-Al_2O_3 (*m*, *n* Refer to Al Coordination Numbers of 4, 5, or 6)

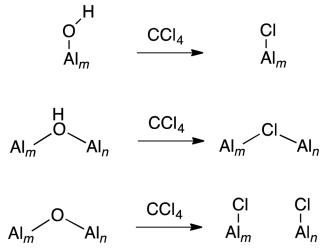

IR spectra of γ-Al_2O_3 and Cl–Al_2O_3 are compared in Figure 2. The unchlorinated support shows the characteristic stretching modes typically assigned to terminal (basic) OH groups at 3790 and 3773 cm^{-1}, while bridging (acidic) OH groups appear at 3730, 3693, and 3676 cm^{-1}.[48] The former tend to be more reactive toward condensation and substitution,[58] and previous theoretical work has shown that the most energetically favorable reaction of γ-Al_2O_3 with HCl involves the replacement of terminal OH groups by Cl.[59] As expected, chlorination of γ-Al_2O_3 leads to major changes in the O–H stretching region of the IR spectrum. The bands attributed to terminal OH groups disappear, while those attributed to bridging hydroxyls are significantly attenuated. A small peak at 3730 cm^{-1} remains visible, as well as a very broad band centered at 3500 cm^{-1} arising from a hydrogen-bonded network. There is no evidence for appreciable amounts of residual H_2O or $AlCl_3$ (Figure S1).[60] The presence of strong Lewis acidity, and the lack of appreciable Brønsted acidity, were verified by pyridine adsorption (Figure S2).

The ^{1}H MAS NMR spectrum of γ-Al_2O_3 (dehydrated and partially dehydroxylated at 450 °C) in Figure 3a consists of two main signals at 1.8 and −0.3 ppm, assigned to doubly bridging (μ^2-OH) and terminal (μ^1-OH) hydroxyl groups, respectively. Chlorination induces significant changes. The ^{1}H MAS NMR

DOI: 10.1021/jacs.6b06953
J. Am. Chem. Soc. 2016, 138, 12935–12947

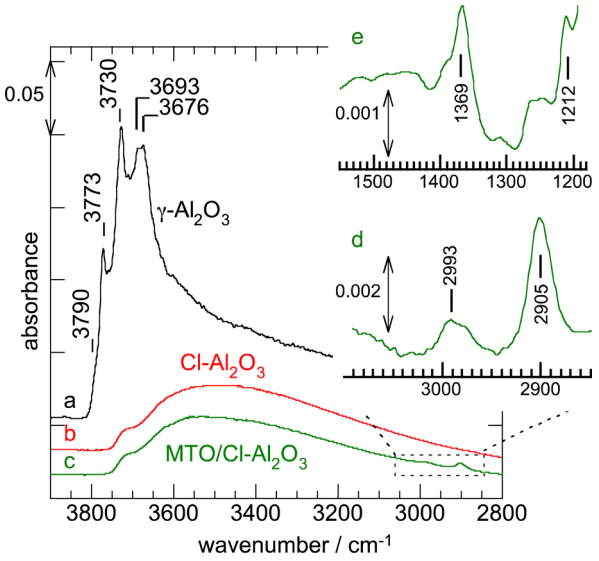

Figure 2. Transmission IR spectra of γ-Al_2O_3: (a) after pretreatment in vacuo at 450 °C (black); (b) after extensive chlorination (Cl–Al_2O_3, 4.0 wt % Cl, red) and subsequent dehydration at 450 °C; and (c) after grafting of MTO (2.5 wt % Re) onto Cl–Al_2O_3 (green). The insets show weak CH_3 stretching (d) and deformation (e) modes (baseline-corrected).

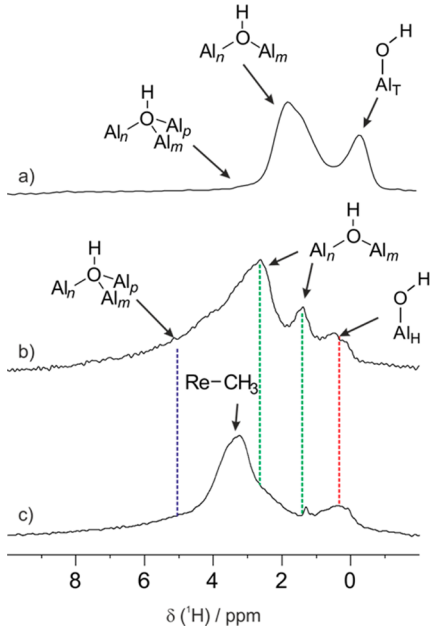

Figure 3. ^{1}H MAS NMR spectra of (a) γ-Al_2O_3 and (b) Cl–Al_2O_3 (4.0 wt % Cl), both dehydrated at 450 °C, as well as (c) MTO/Cl–Al_2O_3 (18.8 T, spinning speed 20 kHz). T and H denote tetra- and hexacoordinated Al, respectively; *m*, *n*, *p* refer to total coordination numbers of 4, 5, or 6. Note: the intensities are not normalized.

spectrum of Cl–Al_2O_3 in Figure 3b comprises three main features: a broad asymmetrical signal with a maximum at 2.6 ppm and extending up to 6 ppm (assigned to μ^2- and μ^3-OH groups), and two weaker but sharper signals at 1.4 and 0.4 ppm.

In order to assign these signals, we resorted to heteronuclear (^{1}H–^{27}Al) solid-state NMR. The ^{1}H–^{27}Al D-HMQC MAS spectrum correlates the ^{27}Al and ^{1}H signals. It confirms the persistence in Cl–Al_2O_3 of tetra-, penta- and hexa-coordinated aluminum sites (denoted Al_T, Al_P and Al_H, respectively), distinguished by their characteristic chemical shift ranges (Figure S3). The main Al_2-μ^2-OH pattern resembles that observed for γ-Al_2O_3 evacuated at 450 °C (Figure S4), but with downfield shifts in the ^{1}H dimension of ca. 1.2 ppm. A significant difference is the disappearance of the characteristic, strongly quadrupolar-coupled signal of the terminal Al_TOH groups (^{1}H: −0.4 ppm). The only type of residual terminal hydroxyl is the Al_HOH, located at 0.4 ppm in the ^{1}H spectrum. The major residual proton-containing sites of Cl–Al_2O_3, namely, the μ^2-OH groups, are correlated with all three types of Al in order of abundance Al_H > Al_T > Al_P. The μ^3-OH groups (^{1}H: 3.5–6 ppm) correlate with Al_H and Al_T, as observed in our previous study of γ-Al_2O_3.[61] Interestingly, the proportion of μ^2-OH sites decreases relative to μ^3-OH sites. These findings demonstrate that the hydroxyl sites most affected by chlorination are μ^1-OH and μ^2-OH sites. The residual hydroxyls have structural types similar to those of γ-Al_2O_3. It has been suggested that some of the strongly interacting hydroxyls are located subsurface,[62] which would make them more resistant to chloride replacement.

Fate of MTO on Cl–Al_2O_3. No methane evolution was detected by either gas phase IR or GC during the grafting procedure. Upon interaction of MTO with Cl–Al_2O_3, new IR bands appear at 2993, 2905, 1369, and 1212 cm^{-1}, Figure 2. The first two are assigned to the asymmetric and symmetric stretching of the methyl group, while the latter two are its asymmetric and symmetric deformation modes. All frequencies are blue-shifted slightly compared to those of crystalline MTO.[24,63] Similar observations have been made for MTO interacting with a variety of oxide supports,[24,27,33,52] and confirm that the methyl group is preserved during grafting. No perturbation of the O–H stretching modes is detected by IR in Figure 2c, suggesting that MTO neither interacts with existing surface hydroxyls nor generates new ones. (Previously, we observed "new" OH stretching intensity in the IR spectrum of MTO/SiO_2–Al_2O_3, but only at high MTO loadings. It was inferred to be caused by H-bonding between pre-existing surface hydroxyls and the oxo ligands of MTO, rather than formation of new OH groups.)[24,25] Vibrations characteristic of either terminal (Re=CH_2) or bridging (Re-CH_2–Al) carbenes are not observed (nor have they been for any other MTO/oxide support combination).

The ^{1}H MAS NMR spectrum of MTO/Cl–Al_2O_3 is presented in Figure 3c. The principal new contribution, which we assign to Re-CH_3, is centered at 3.3 ppm. ^{1}H–^{1}H DQ-SQ MAS NMR confirms this assignment, since intense on-diagonal signals are indeed observed from 3.1 to 3.9 ppm, Figure S5. The chemical shift for the most abundant Re site reflects changes in metal coordination that induce significant methyl deshielding relative to that of molecular MTO in $CDCl_3$ (2.64 ppm).[24] A second, weaker methyl signal is present at 2.9 ppm according to the ^{13}C–^{1}H HETCOR (see Figure 5 and the corresponding discussion below), although it is not resolved in Figure 3. Its chemical shift is similar to that of MTO/SiO_2–Al_2O_3 (2.8 ppm)[24] and MTO/γ-Al_2O_3 (2.6 ppm, Figure S6). There is no evidence for either Re-CH_2–Al (expected at ca. 9 ppm)[64] or Re=CH_2 (expected at 13–14 ppm).[65]

Comparison to the ^{1}H MAS NMR spectrum of Cl–Al_2O_3 (Figure 3b) shows how MTO grafting perturbs the hydroxyl network. The main change is the attenuation of the signal at 1.4 ppm, assigned to μ^2-OH. The other μ^2-OH groups (2.5–8.5 ppm, with extremely long relaxation times) are relatively unperturbed, as is the broad signal centered at 0.4 ppm, due to

DOI: 10.1021/jacs.6b06953
J. Am. Chem. Soc. 2016, 138, 12935–12947

residual μ^1-OH sites. The ^{1}H−^{1}H DQ-SQ MAS NMR spectrum of MTO/Cl−Al_2O_3 shown in Figure S5 reveals correlations within the hydroxyl network reminiscent of γ-Al_2O_3 (e.g., proximity of different types of μ^2-OH groups, and of μ^2-OH and μ^3-OH; self-correlation of μ^1-OH).[61] This indicates that part of the surface of Cl−Al_2O_3 retains the structure of γ-Al_2O_3. MTO grafted in these regions appears to interact with μ^2-OH groups selectively, among the various types of surface hydroxyls amenable to observation (manifested in the decreased signal intensity at 2.5 and 1.4 ppm relative to that of the 0.4 ppm signal assigned to Al_HOH). The broader implications of this observation will be the subject of future investigations.

The 2D ^{1}H−^{27}Al D-HMQC MAS NMR spectrum of MTO/Cl−Al_2O_3 is shown in Figure 4. It shows two remarkably distinct, major patterns. The first, in the range 1.5−3.5 ppm in the ^{1}H dimension, is due mostly to μ^2-OH. The μ^3-OH signals (^{1}H: 3.5−6 ppm) correlate with Al_H and, to a lesser extent, Al_T. The regions of Cl−Al_2O_3 that are largely unaffected by grafting are highlighted by the dashed rectangles in Figure 4. These signals are partially masked by the second major pattern (solid rectangle in Figure 4). It includes the ^{1}H chemical shifts of Re−CH_3, and correlates with all three types of Al (relative proportions: $Al_H \approx Al_T > Al_P$). Careful analysis of the ^{1}H dimension in the Re-CH_3 region shows that the low chemical shift region correlates with Al_T/Al_H, the high chemical shift region with Al_P/Al_H. In the light of the analysis below, these pairwise correlations suggest strong interactions between Re and a *bridging* oxygen (Al_nOAl_H, n = T or P) of the surface (see proposed structure in Scheme 3).

The ^{13}C cross-polarization (CP) MAS spectrum of ^{13}C-labeled MTO supported on Cl−Al_2O_3 consists of a broad signal between 25 and 50 ppm, with two resolved maxima at 30 and 37 ppm, Figure 5a. It is strikingly simple compared to the

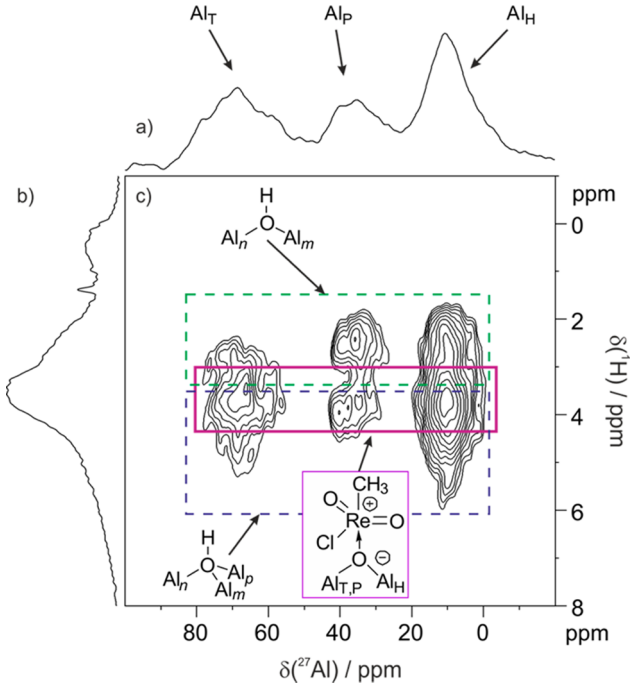

Figure 4. Solid-state NMR of MTO/Cl−Al_2O_3: (a) ^{27}Al projection, (b) ^{1}H MAS, and (c) ^{1}H−^{27}Al D-HMQC MAS NMR (18.8 T, spinning speed 20 kHz, recycle delay 2 s, recoupling time 500 μs).

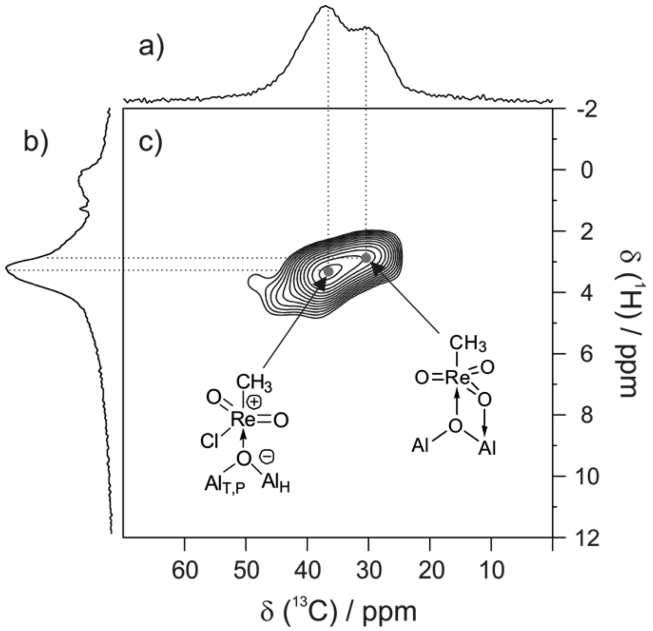

Figure 5. (a) ^{13}C CP MAS, (b) ^{1}H MAS NMR, and (c) ^{13}C−^{1}H HETCOR spectra of MTO supported on Cl−Al_2O_3 (2.4 wt % Re; 4.0 wt % Cl; (a, c) 7.05 T, spinning rate 10 kHz; (b) 18.8 T, spinning rate 20 kHz.

complex spectrum of MTO on unmodified γ-Al_2O_3 (Figure S7). ^{1}H−^{13}C HETCOR confirms the presence of two CH_3 environments in MTO/Cl−Al_2O_3, Figure 5c. The minor ^{13}C signal, at 30 ppm (corresponding to the ^{1}H signal at 2.9 ppm), is assigned to MTO coordinated to Lewis acid sites, and is similar to signals reported on both SiO_2−Al_2O_3 and γ-Al_2O_3.[24,52] Proposed structures for this site are shown in Scheme 2, where the multiple Lewis acid−base interactions resemble those found for ReO_4^- interacting with SiO_2−Al_2O_3 and γ-Al_2O_3.[66] Since the ^{13}C chemical shift of MTO is just 19 ppm in $CDCl_3$,[63] it is apparent that the interactions with Lewis acid sites result in strong downfield shifts. The major ^{13}C signal, at 37 ppm (corresponding to the ^{1}H signal at 3.2 ppm), has not been reported previously, and is presumably associated with the new Re sites present on Cl−Al_2O_3. Although CP-MAS NMR is not fully quantitative, we estimate the relative proportion of the two sites to be ca. 70:30 in favor of the new signal (Figure S8).

Finally, we considered whether the higher ^{1}H chemical shift of the protons in MTO grafted on Cl−Al_2O_3 relative to molecular MTO could indicate formation of a "$ReOCH_3$" site. A methoxide should also give rise to ^{13}C NMR signals in the range 65−75 ppm,[68,69] where we observe no such signals. Curiously, a ^{13}C signal was reported at 64−65 ppm for MTO/

Scheme 2. Previously Proposed Structures, with Observed NMR Chemical Shifts, for Intact MTO Grafted onto SiO_2−Al_2O_3 (A)[25] and γ-Al_2O_3 (B),[52,67] as Well as a Proposed Methylene-Bridged Structure on γ-Al_2O_3 (C)[52,67]

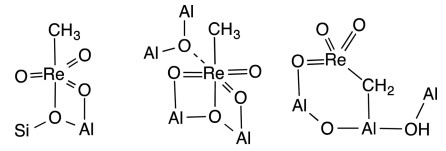

DOI: 10.1021/jacs.6b06953
J. Am. Chem. Soc. 2016, 138, 12935−12947

γ-Al_2O_3, where it was assigned[52] to a bridging methylene [Re-CH_2−Al] arising from spontaneous methyl tautomerization (represented by structure C in Scheme 2). This possibility can be completely excluded for MTO/Cl−Al_2O_3 based on the ^{13}C and ^{1}H NMR spectra (Figures 3c and S7), since there are no signals in the corresponding regions. Hence, only Re-CH_3 groups are present in detectable quantities, consistent with the IR spectrum in Figure 2.

Coordination Environment of MTO Grafted onto Cl−Al_2O_3. The nature of the ligands bound to Re in MTO/Cl−Al_2O_3 was investigated by analysis of the Re *L*-edge X-ray absorption spectrum. The Re L_I- and L_{III}-edge energies (12 539 and 10 540 eV, respectively),[70,71] as well as the intense whiteline at the Re L_{III}-edge,[71,72] are consistent with the presence of Re(VII) (Figures S9 and S10). The strong pre-edge feature at the Re L_1-edge implies the absence of an inversion center.[66,71] The Re L_{III}-edge EXAFS shows a broad peak between 1.0 and 1.5 Å in *R*-space, very similar to the spectrum of MTO/γ-Al_2O_3 (Figure 6a), as well as to spectra reported for MTO/SiO_2−Al_2O_3,[24] and MTO/zeolite Y.[73] It arises due to scattering by light atoms (C, O) located in the first coordination sphere of Re. However, for MTO/Cl−Al_2O_3, the intensity of this peak is significantly suppressed, Figure 6b, consistent with fewer light atoms and/or more extensive destructive interference between these paths. In addition, there is a prominent new feature at ca. 2 Å, whose location and intensity suggest a heavier scatterer, such as Cl.

In spite of evidence for severe heterogeneity in MTO/γ-Al_2O_3 based on the ^{13}C CP-MAS spectrum NMR (Figure S7), a successful EXAFS curve fit was achieved using a very simple model, Figure S11. Three short Re═O bonds have an average distance of 1.721 Å, Table 2. A longer Re−O path was combined with the Re−C path because of their similar distances and scattering amplitudes, resulting in an average distance of 2.14 Å. The long Re−O interaction presumably involves an oxygen associated with γ-Al_2O_3 (as in Scheme 2, structures A and B), but the distance is much shorter (and chemically more plausible) than a previously reported value (2.47 Å).[52] Because the average long Re−C/O distance reflects contributions from two slightly different paths, we cannot infer a significant elongation of the Re−C bond relative to CH_3ReO_3 (2.06 Å).[63] There is no evidence for an even longer Re−O path (structure B), but a nonbonded Re−Al single-scattering path was successfully refined at 3.13 Å, comparable to the distance reported earlier for MTO interacting with the Lewis acidic Al sites of SiO_2−Al_2O_3 (structure A).[24] The distance is physically reasonable, and the weak intensity is expected for a relatively long scattering path in a heterogeneous material.

For MTO/Cl−Al_2O_3, a satisfactory curve fit was obtained using a two-site model that accounts for the presence of two different Re species, as required by the ^{13}C CP-MAS NMR spectrum (Figure 5). The first site is the same one used to fit the EXAFS of MTO/γ-Al_2O_3, while the second site has undergone O−Cl exchange. In order to limit the number of variables in the fit, the fractional contributions of the two sites were correlated by the parameter α, representing the number of oxo ligands exchanged for chloride. Thus, α represents the fraction of grafted MTO interacting with Lewis acid sites on γ-Al_2O_3 unperturbed by the presence of Cl, while (1-α) represents the fraction of sites with a Re−Cl path.

The curve fit is shown in Figure 6c (*R*-space) and Figure S12 (*k*-space), with curve fit parameters in Table 2. The two contributing sites have the same Re═O distance, 1.69 Å, which is insignificantly different from that of molecular MTO (1.71 Å),[63] and comparable to values reported here and in the literature[24,52] for MTO grafted onto both SiO_2−Al_2O_3 and γ-Al_2O_3. Similarly, the Re−C distance, 2.08 Å, is hardly affected by the surface interaction or by the presence of chloride. The fraction of sites bearing a chloride ligand, (1-α), is 0.5. Considering the typical uncertainty in EXAFS coordination numbers (ca. 20%), this value is consistent with the estimated 70% abundance of the new site according to ^{13}C CP-MAS NMR (peak at 37 ppm, Figure 5a). In both contributing sites, the interaction of MTO with the support appears to involve a long Re−O path (combined in the fit with the Re−C path due to their similar distances). Thus, the curve fit supports the presence of a major new species derived from MTO, identified as [$CH_3ReO_2Cl^+$]. The long Re−O distance attributed to the surface interaction (ca. 2.08 Å) is intermediate between that expected for an anionic alkoxide ligand and a neutral ether ligand (e.g., 1.859 and 2.323 Å, respectively, in [$ReO_3(\kappa^2$-$OC(CH_3)_2)C(CH_3)_2OCH_3)$]).[74] It is consistent with adsorption of a formally cationic [$CH_3ReO_2Cl^+$] fragment at an anionic [Al−O−Al$^-$] site.

At 2.33 Å, the short Re−Cl distance is characteristic of a terminal Re−Cl bond. The analogous bond distances in $ReOCl_4$ and $ReOCl_4$(THF) are 2.26 and 2.30 Å, respectively.[75,76] Longer Re−Cl bonds may reflect increased steric crowding, as in $ReO_3Cl(THF)_2$ (2.43 Å), or an anionic complex, as in $CH_3ReO_3Cl^-$ (2.63 Å).[77] Bridging chlorides in well-defined molecular complexes exhibit significantly longer distances as well: for example, 2.54 Å for a complex with a

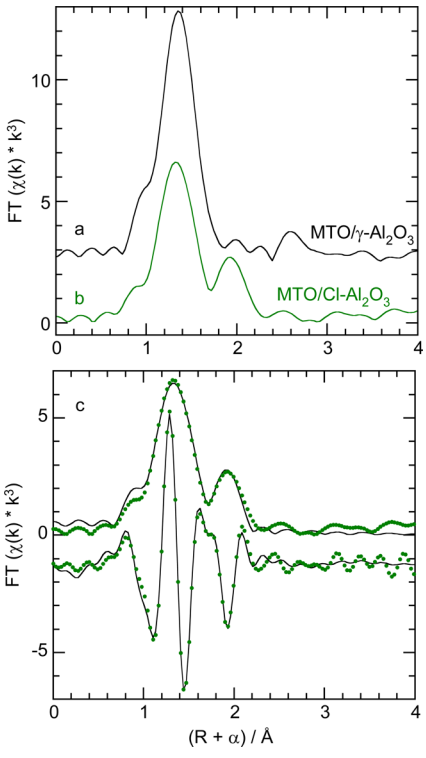

Figure 6. Comparison of EXAFS FT magnitudes in k^3-weighted, nonphase-corrected *R*-space, for MTO grafted onto (a) γ-Al_2O_3 (2.4 wt % Re, black), or (b) Cl−Al_2O_3 (2.4 wt % Re, 4.0 wt % Cl, green). Spectra are displayed on the same *y*-scale, but are offset vertically for clarity. (c) Curve-fit (lines) of the EXAFS data for MTO/Cl−Al_2O_3 (points), is shown for both the imaginary component and the FT magnitude, with curve-fit parameters in Table 2.

DOI: 10.1021/jacs.6b06953
J. Am. Chem. Soc. 2016, 138, 12935−12947

Table 2. Curve-Fit Parameters[a] for the Re L_{III}-Edge EXAFS of Supported MTO

catalyst	path	N[b]	R (Å)	$10^3\ \sigma^2$ (Å^2)
MTO/γ-Al_2O_3	Re=O	3	1.721 (0.004)	2.4 (5)
	Re−C/O	2	2.14 (0.01)	4 (1)
	Re−Al	1	3.13 (0.03)	6 (3)
MTO/Cl−Al_2O_3	Re=O	2.5 (0.1)	1.69 (0.01)	3 (1)[c]
	Re−C/O	2	2.08 (0.04)	9 (5)
	Re−Cl	0.5 (0.1)	2.33 (0.02)	3 (1)[c]

[a] S_0^2 and ΔE_0 were refined as global fit parameters, returning values of (0.9 ± 0.4) and (3.9 ± 1.9) eV, respectively for MTO/γ-Al_2O_3 ($2.4 \le k \le 14$ Å^{-1}; $1.0 \le R \le 3.3$ Å), and (0.90 ± 0.08) and (0 ± 1) eV, respectively, for MTO/Cl−Al_2O_3 ($3.0 \le k \le 14.0$ Å^{-1}; $1.0 \le R \le 2.4$ Å). [b] For the single-site model used to represent MTO/γ-Al_2O_3, all coordination numbers (N) were fixed at integer values, to give physical meaning to σ^2 values. For the two-site model used to represent MTO/Cl−Al_2O_3, coordination numbers were constrained as follows: $N_{Re=O} = (2+\alpha)$; $N_{Re-C/O} = (2)$; $N_{Re-Cl} = (1-\alpha)$. [c] Constrained to the same value.

[Re(μ-Cl)(μ-CO)Zn] core,[78] and 2.71 Å for a complex with a [Re_2(μ-Cl)$_2$] core.[79] We were unable to refine a long Re−Al path, suggesting that the bridging interaction is nonrigid (in contrast to Re(μ-X)$_2$Al, X = O and/or Cl). In the absence of such rigidity, variability in the Re−Al distance between sites would result in destructive interference between single-scattering paths and suppression of the EXAFS intensity.

Ligand Exchange on Cl−Al_2O_3. The spectroscopic characterization results described above suggest a profound modification of MTO as a result of its interaction with Cl−Al_2O_3. For example, the EXAFS indicates the presence of two different Re-containing species: (1) intact MTO, interacting via the oxo ligands with Lewis acid sites present on the γ-Al_2O_3 surface (similar to structure A in Scheme 2), and (2) a chlorinated version, interacting via Re with Lewis basic sites. However, the short Re−Cl distance (2.33 Å) and decreased number of short Re=O paths in the second site are not consistent with chloride abstraction leading to [CH_3ReO_3Cl]$^-$, but rather with chloro-oxo ligand exchange leading to a supported [$CH_3ReO_2Cl^+$] fragment interacting with an anionic surface oxygen. There is ample literature precedent for chloride abstraction in the molecular chemistry of Re complexes, including the reaction of perrhenate with $(CH_3)_3SiCl$ in THF to give [$ReO_3Cl(THF)_2$],[75] and the reaction of Re_2O_7 with thionyl chloride to give [$ReO_3Cl]_2(SO_2Cl_2)$].[80] In the presence of stabilizing Lewis bases and PPh_3, MTO has been shown to abstract chloride from $(CH_3)_3SiCl$ *and* eliminate an oxo ligand, as O=PPh_3.[81,82] Such reactions may resemble the reactions of MTO with Cl−Al_2O_3. It is also relevant to this work that, while solutions of MTO alone do not catalyze olefin metathesis, their "activation" by $AlCl_3$[83] likely involves Cl−O exchange.[21]

Proposed structures for the grafted sites based on the preponderance of spectroscopic evidence are shown in Scheme 3. Coordination of intact MTO to unchlorinated regions of the surface via multiple Lewis acid−base interactions, as in species D, is associated with the ^{13}C NMR signal at 30 ppm, by analogy to structure A (Scheme 2). Its long Re−O(Al) and rigid Re−Al paths are consistent with the EXAFS. Coordination of MTO to a chlorinated region of the surface results in Cl−O exchange, affording species E. In accord with the EXAFS, this site features a short Re−Cl bond, a long Re−O bond, and no well-defined Re−Al path. It is tentatively associated with the new ^{13}C NMR signal at 37 ppm (supported by DFT calculations, see below). The proposed ligand exchange leading to E is reminiscent of observations made with early olefin metathesis systems based on tungsten. For example, [$W(OCH_2{}^tBu)_2(CH_2{}^tBu)_2$] reacts with $AlCl_3$ to form a bimetallic adduct [$W(OAlCl_3)(OCH_2{}^tBu)_2(CH_2{}^tBu)_2$] featuring a W−O−Al bridging interaction,[84] which evolves to [$W(OCH_2{}^tBu)_2(CH{}^tBu)Cl_2$] and generates "$(AlOCl)_n$" as an incompletely characterized side-product.[85]

Scheme 3. Structures Proposed in This Work, and Their Assigned NMR Signals, for MTO Interacting with Unchlorinated (D) and Chlorinated (E) Regions of the Cl−Al_2O_3 Surface

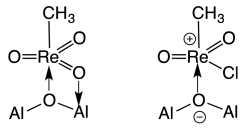

To confirm the exchange of oxygen for chloride at Re=O, we grafted ^{17}O-enriched MTO onto Cl−Al_2O_3 and characterized the resulting material by ^{17}O MAS NMR. The chemical shift of Re=O is observed at ca. 800 ppm, Figure S13a, consistent with the reported value for MTO (803 ppm).[86] The spectrum of MTO/Cl−Al_2O_3 in Figure S13c is devoid of such signals. However, supported metal-oxo species can be difficult to observe by solid-state ^{17}O MAS NMR, due to their large chemical shift anisotropies, and the presence of a distribution of sites which further broadens signals and prevents their efficient observation.[87] Nevertheless, a signal is visible at 13 ppm, with a shoulder at 50 ppm. Both are assigned to oxygen associated with the alumina support, i.e., Al−O-X (X = Al, H), by comparison to the spectrum of ^{17}O-enriched γ-Al_2O_3 (Figure S13b). The appearance of these signals is consistent with the proposed ligand exchange between Re=^{17}O and Al−Cl, resulting in ^{17}O incorporation into the alumina surface.

Impact of Chlorination on Catalyst Stability. To investigate the impact of chlorination on catalyst lifetime, a flow reactor study was performed with 1 bar propene at 10 °C. The flow rate was adjusted to 1.92 mol C_3H_6 s^{-1} (mol Re)$^{-1}$ to ensure less than equilibrium conversion (33.7%),[88] in order to assess catalyst deactivation. The TOF measured at 15−20 min on-stream for MTO/Cl−Al_2O_3 is 0.57 s^{-1}, which is approximately three times higher than that of MTO/γ-Al_2O_3 under the same conditions (0.20 s^{-1}). This activity enhancement is consistent with the batch reactor results in Figure 1, although the difference is clearly more pronounced at the much shorter reaction times sampled in the batch reactor.

Figure 7 compares cumulative turnovers (TON) for the two catalysts. After 37 h on-stream, TON for MTO/γ-Al_2O_3 reached a plateau at 4.6×10^3, while the value for MTO/

DOI: 10.1021/jacs.6b06953
J. Am. Chem. Soc. 2016, 138, 12935−12947

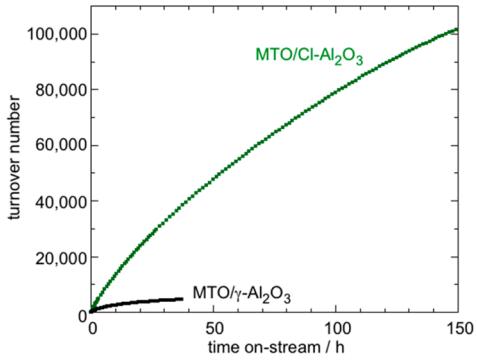

Figure 7. Comparison of productivity for MTO/Cl−Al_2O_3 (green) and MTO/γ-Al_2O_3 (black), in propene metathesis in a flow reactor. Conditions: 10 °C, 1 bar, 1.92 mol $C_3H_6 \cdot s^{-1} \cdot (\text{mol Re})^{-1}$.

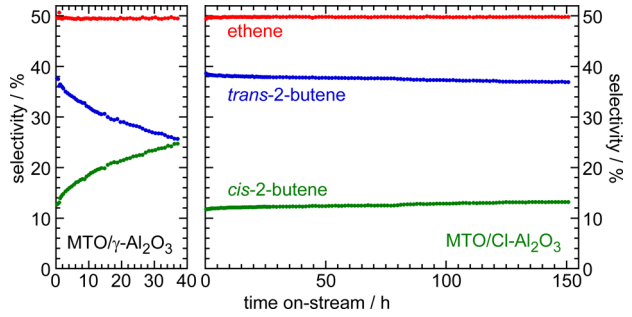

Figure 8. Selectivity comparison of selectivity during propene metathesis catalyzed by MTO/γ-Al_2O_3 (left) and MTO/Cl−Al_2O_3 (right), in a flow reactor. Conditions: 10 °C, 1 bar, 1.92 mol $C_3H_6 \cdot s^{-1} \cdot (\text{mol Re})^{-1}$.

Cl−Al_2O_3 was an order of magnitude higher (38×10^3). After 150 h, TON for the Cl-promoted catalyst exceeded 1.0×10^5, and was still rising when the test ended after 150 h. For MTO/γ-Al_2O_3, the activity decreased rapidly: conversion declined from its initial value of 10% to less than 3% after just 5 h on-stream (Figure S14). At the end of the test (after 37 h), the conversion was 0.6%. In contrast, the more active MTO/Cl−Al_2O_3 catalyst initially shows ca. 30% conversion, declining to 10% (i.e., equivalent to the initial activity of MTO/γ-Al_2O_3) only after 60 h. Even after 150 h, the conversion remained above 5%. The stability of the MTO/Cl−Al_2O_3 catalyst is exceptional, relative to all other reports for supported Re-based catalysts. A stronger interaction of MTO with the chlorinated regions of Cl−Al_2O_3 may retard bimolecular deactivation processes, but it is also likely that the absence of nearby Brønsted acidic sites prevents deactivation by protonolysis. In contrast, the level of surface dehydroxylation apparently does not affect either the activity or the number of active sites for propene metathesis in MTO/γ-Al_2O_3 catalysts when the support is thermally pretreated in vacuum at temperatures between 500 and 1000 °C.[89] Thus, the enhanced performance of MTO/Cl−Al_2O_3 is a direct consequence of chlorination, and not an indirect result of the dehydroxylation that accompanies this modification of the support.

For both MTO/γ-Al_2O_3 and MTO/Cl−Al_2O_3, the metathesis products are comprised of equimolar amounts of ethene and 2-butenes. The evolution of the *trans*/*cis* isomers of 2-butene provides further confirmation of catalyst stability. In olefin metathesis, stereoselectivity arises due to differences in the relative stabilities of metallacyclobutanes.[90] Thus, the [1*e*,2*e*] isomer, with two adjacent methyl substituents in equatorial positions in the metallacyclobutane ring, is energetically favored over the [1*e*,2*a*] isomer, with one equatorial and one axial methyl substituent, Scheme S1. At low conversion, there is a kinetic preference for *cis*-2-butene arising from the [1*e*,2*e*] intermediate, while at higher conversion, further metathesis results in via *cis*−*trans* isomerization which causes the ratio to approach its thermodynamic value (4.4 at 10 °C).[91] Consequently, the *trans*/*cis* ratio tends to decrease as a function of time on-stream due to catalyst deactivation. The evolution of the *trans*/*cis* ratios in the 2-butene products with time on-stream is compared for MTO/γ-Al_2O_3 and MTO/Cl−Al_2O_3 in Figure 8. Severe deactivation of MTO/γ-Al_2O_3 is accompanied by a rapid decrease in the *trans*/*cis* ratio of the 2-butenes as the experiment proceeds, starting at 3.0 but eventually stabilizing at 1.0 after 37 h. For MTO/Cl−Al_2O_3, the initial ratio is 3.3, and is still 2.4 even after 150 h. This is consistent with higher conversion throughout the experiment compared to the nonchlorinated catalyst, and agrees with results reported for other d^0 catalyst systems.[92−100] Thus, the high activity and stability of MTO/Cl−Al_2O_3 do not come at the expense of stereoselectivity.

Computational Investigation of Ligand Exchange between MTO and Al_2Cl_6. We performed DFT calculations for some proposed surface species, in order to test our assignments of their ^{13}C and ^{1}H NMR shifts, to corroborate our EXAFS and ^{17}O NMR results, and to provide preliminary evidence of thermodynamic plausibility of Cl−O ligand exchange. While several periodic[59,101,102] and cluster[103−105] computational models for the various facets of partially dehydroxylated γ-Al_2O_3 surfaces have been proposed, their relevance to high surface area aluminas remains controversial,[106,107] and there is as-yet no direct experimental evidence[62,108] for a key structural feature of these computational models, i.e., highly coordinatively unsaturated tricoordinate Al atoms, which calculations have deemed responsible for their ability to activate MTO.[89] Structural models for the surface of chlorinated alumina are even less well-developed. Digne et al. constructed a periodic model,[54] but incorporated Cl only in terminal positions replacing nonbridging hydroxyl groups. They pointed out that more extensive chlorination must involve the formation of "$AlCl_3$"-like domains via strong surface reconstruction.

Since none of the model systems described above are consistent with a heavily chlorinated and likely reconstructed alumina surface, our calculations used an extremely simple Al_2Cl_6 cluster instead. As is the case for computational models of γ-Al_2O_3, it is not clear that this cluster geometry is representative of the highly chlorinated regions of an Al_2O_3 surface, whose oxygen content is greatly reduced. However, the structure of $Al_2(\mu\text{-}Cl)_2Cl_4$ does include both bridging and terminal chlorides (Figure S15 and Table S1). While we are aware that we cannot properly model the chlorinated alumina surface with this compound, it is nevertheless possible (particularly in the absence of a more sophisticated model for the surface of chlorinated alumina) to use it to confirm reactivity patterns regarding the oxo-chloride exchange chemistry proposed here on the basis of experimental evidence. It is noteworthy that Al_2Cl_6 has been shown to activate MTO for olefin metathesis in solution,[83] likely via oxo-chloride ligand exchange.[21]

Scheme 4 shows the structures and relative free energies of two adducts **Ia** and **IIa** between MTO and Al_2Cl_6 in which a

DOI: 10.1021/jacs.6b06953
J. Am. Chem. Soc. 2016, 138, 12935−12947

bridging Cl ligand and a terminal oxo ligand have been exchanged between Al and Re to give structures with a bridging O ligand between Al atoms and terminal Re−Cl bond, consistent with the EXAFS and ^{17}O NMR results described above. An investigation of alternative adducts with Re−O−Al bridges and no Re−Cl bonds yielded higher free energy structures (**IIIa**, **IVa**, and **Va** in Scheme S2), and no stable structures with a Re−Cl−Al bridge. In structure **Ia**, oxo ligands of the (formally anionic) $[CH_3ReO_3Cl^-]$ fragment form bridges to two Al sites of the $[Al_2Cl_5^+]$ cluster, resulting in a slight elongation of the Re−O distances (to ca. 1.80 Å, Table S2). In structure IIa, the (formally cationic) $[CH_3ReO_2Cl^+]$ fragment interacts with a bridging oxygen of the $[Al_2Cl_5O^-]$ cluster, resulting in a single, long Re−O distance of length 1.94 Å which approximately matches the value obtained in the EXAFS curve fit.

Scheme 4. DFT-Optimized Structures for MTO after Ligand Exchange with Al_2Cl_6, with Computed NMR Chemical Shifts, for Both Methyl and Methylene Tautomers[a]

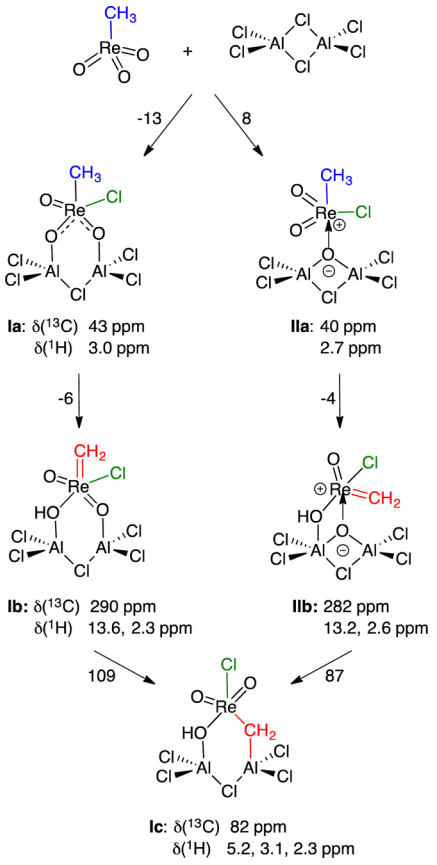

[a]Numbers beside the arrows represent standard free energy changes in kJ/mol, computed at 298 K.

The calculated ^{13}C NMR chemical shifts for species **Ia** and **IIa** (43 and 40 ppm, respectively) occur at higher frequencies compared to those of the O-bound adducts **IIIa**, **IVa** and **Va** without Re−Cl bonds ($27 \leq \delta \leq 35$ ppm, Scheme S2). The predicted difference, while small, corroborates the assignments for the experimentally observed shifts of 37 and 30 ppm for the chlorinated and unchlorinated Re sites of MTO/Cl−Al_2O_3, respectively (Figure 5a). The predicted ^1H signals of **Ia** and **IIa** (Table S3) also shift to slightly higher frequencies, as observed experimentally (Figure 4).

While the predicted spectra and structures of **Ia** and especially **IIa** corroborate several experimental observations, **Ia** is predicted to be slightly more stable than **IIa**. We assign no significance to the small difference in computed adsorption energies; we emphasize that Al_2Cl_6 is an extremely simple model and is unlikely to predict adsorption energies for chlorinated alumina accurately. At best, the model demonstrates that structures **Ia** and **IIa** are plausible, with **IIa** being consistent with more of the spectroscopic evidence than **Ia**.

Origin of the Initiating Carbene Ligand. We also used DFT to examine carbene formation by tautomerization, involving proton transfer from the methyl ligand to an oxygen associated with the chlorinated Re sites. Tautomerization by proton transfer from the methyl group in free MTO to an oxo ligand of Re is prohibitively far uphill.[109] However, proton transfer to one of the bridging oxygens (AlORe) of **Ia** to give **Ib** is nearly isoenergetic (Scheme 4). Likewise, proton transfer from the methyl group in **IIa** to create a bridging hydroxyl in **IIb** (bond lengths in Table S7) is nearly isoenergetic. In contrast, proton transfer to a terminal oxo ligand of Re to give a terminal hydroxyl is highly unfavorable for MTO on the Al_2Cl_6 cluster, with or without Cl ligand exchange (Scheme S3).

Since MTO/Cl−Al_2O_3 appears to have a much higher fraction of active sites than other supported MTO-based metathesis catalysts (vide supra), we sought further evidence for the appearance of a carbene ligand under reaction conditions, using ^{13}C NMR spectroscopy. Typical ^{13}C NMR chemical shifts for terminal Re alkylidenes lie in the range 250−310 ppm, and the unstable methylidene complex $[Re(=CH_2)(CH_2{}^tBu)(\equiv C{}^tBu)(bpy)OTf]$ has a ^{13}C chemical shift of 258 ppm in C_6D_6.[65] The computed values for methylidenes **Ib** and **IIb** are similar (Scheme 4). When MTO/Cl−Al_2O_3 was treated with $CH_3{}^{13}CH{=}CH_2$ (70 mbar at 0 °C for 60 min), a ^{13}C signal was observed at 246 ppm by CP/MAS NMR (Figure S16). However, a blank experiment without MTO confirmed that the signal is present when propene adsorbs on Cl−Al_2O_3. A similar signal observed when propene was adsorbed on HY zeolite was assigned to a methyl-substituted cyclopentenyl cation.[110] It is therefore unlikely to be the signal for a terminal carbene on Re.

Supported analogues of **Ib** and **IIb**, if present, are therefore not abundant enough to be spectroscopically observable. In studies of MTO/γ-Al_2O_3, it has been suggested that they rearrange to give dormant, bridging methylidenes (Scheme 2, structure **C**).[52] However, the absence of any IR, ^{13}C NMR, or ^1H NMR signals for such species in the much more active MTO/Cl−Al_2O_3 catalyst demonstrates that bridging carbenes are not present here either, nor is there a reason to invoke highly energetic tricoordinate aluminum sites to form them.[89] This finding is consistent with previous experimental results for the very active MTO/SiO_2−Al_2O_3 catalyst,[25] and with our DFT predictions that conversion of either **Ib** or **IIb** to **Ic** is significantly uphill (Scheme 4). Finally, our DFT calculations show that terminal methylidenes are less stable than the corresponding rhenacyclobutane intermediates formed in their reactions with C_2H_4 or C_3H_6, Scheme S4, therefore the metallacycles are the likely resting states under reaction conditions. Since calculated ^{13}C chemical shifts for the rhenacyclobutanes lie in the region 20−50 ppm, they are difficult to distinguish from signals for adsorbed olefins and oligomers (Figure S16).

DOI: 10.1021/jacs.6b06953
J. Am. Chem. Soc. 2016, 138, 12935−12947

CONCLUSIONS AND PERSPECTIVES

MTO adsorbed on chlorinated alumina, which simultaneously supports and activates the organometallic fragment, is the first example of a highly active and long-lived low temperature Re-based heterogeneous metathesis catalyst. The increased fraction of active sites and increased per-site activity measured at short reaction times, as well as the increased overall activity and stability measured at long reaction times, in conjunction with spectroscopic measurements which indicate a high degree of site uniformity, require that the active sites differ both quantatively *and qualitatively* from those of previously reported supported catalysts based on oxides of Re and their organometallic derivatives. They are also valuable for being simple to prepare, with no need for exotic spectator ligands, or even for a preinstalled carbene. These are major advances for supported Re-based metathesis catalysts, for which wider industrial implementation has been severely hampered by stability issues.

A variety of complementary spectroscopic techniques (IR, multinuclear solid-state NMR, and X-ray absorption), with additional support from DFT modeling, demonstrate that the coordination environment of MTO is modified by its grafting onto $Cl-Al_2O_3$, although the methyl group initially remains intact. Formulation of a new site as cationic $[CH_3ReO_2Cl^+]$ interacting with an anionic $[AlOAl^-]$ surface site formed by ligand exchange between MTO and the chlorinated alumina surface (Scheme 5) is consistent with the experimental and computational evidence presented above. The activation of MTO by $Cl-Al_2O_3$ thus bears a resemblance to single-site olefin polymerization catalysts, in which ligand exchange with a Lewis acidic cocatalyst generates an electrophilic (usually, cationic and coordinatively unsaturated) active site.[111] Interestingly, Lewis acids such as $AlCl_3$, $GaBr_3$ and $B(C_6F_5)_3$ are also known as cocatalysts for molecular metathesis precatalysts of Mo, W and Re, both "classical" (formed in situ) and "well-defined" (isolated as alkylidenes).[112−116] In many of these systems, the cocatalyst has been suggested to perturb the active site electronic structure via halide ligand substitution, and/or coordination of the Lewis acid to an oxo ligand, in addition to ligand abstraction.

Scheme 5. Proposed Activation of MTO by $Cl-Al_2O_3$

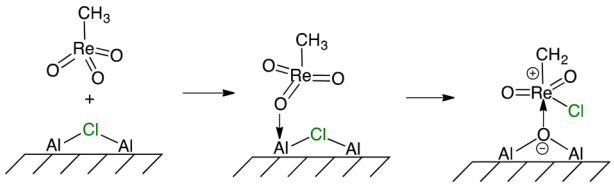

The discovery of a heterogeneous metathesis catalyst that is both highly active and productive at low temperatures suggests new directions in the development of effective catalysts for the metathesis of nonvolatile and functionalized olefins. In particular, there is evidence that chlorination enhances the activity of other types of heterogeneous metathesis catalysts, including those based on perrhenates and molybdates.[14,45,46] We note that halogenated oxides have already proven to be effective support-activators for single-site olefin polymerization catalysts.[117,118]

EXPERIMENTAL METHODS

Catalyst Preparation. The γ-Al_2O_3 (Strem, BET surface area ca. 200 $m^2\ g^{-1}$) was calcined at 450 °C in air for 4 h, then evacuated at the same temperature under dynamic vacuum (0.1 mbar) overnight. This partially dehydrated and dehydroxylated alumina was chlorinated in a stream of CCl_4-saturated N_2 (Praxair, 99.5%, 10 mL/min) in a fixed-bed reactor at 300 °C for 1 h. The resulting $Cl-Al_2O_3$ was evacuated at 200 °C for 3 h, then at 450 °C overnight. Both unchlorinated and chlorinated aluminas were modified with MTO (98%, Sigma-Aldrich) by sublimation into the reactor at room temperature and 0.0001 mbar. Periodically, the solid was shaken vigorously to promote uniform deposition of MTO. After grafting, the catalyst was evacuated overnight at room temperature to remove physisorbed material.

Re loadings were determined by quantitative extraction, followed by UV spectrophotometric analysis as described previously.[24] Cl loading was quantified using bomb combustion/ion chromatography by Columbia Analytical (Tucson, AZ).

Active Site Counting. The number of active sites was evaluated in a 120 mL batch reactor, according to a previously described method.[51] There is considerable uncertainty involved in this measurement, due to strong retention of olefins on the surface: thus, insufficiently long evacuation times can lead to overestimation of the active site count, while excessive evacuation times may undercount them as a result of decomposition of the active sites. Consequently, trends are only significant for materials subjected to identical measurements, and absolute values should be regarded with caution. In a typical, optimized procedure, a 100 mg sample was loaded into the reactor inside an Ar-filled glovebox. After evacuation and cooling to 0 °C, 2-butenes (160 mbar, mixture of *cis/trans* isomers, Sigma-Aldrich, ≥99%) were admitted into the reactor and allowed to react for 3 h. Following evacuation at room temperature for 30 min, the addition of 2-butenes was repeated to ensure complete reaction. After evacuation at room temperature overnight, ethene (160 mbar, Praxair, containing 0.5% propane as internal standard) was introduced into the reactor and allowed to react for 3 h at 0 °C. The amount of propene released was analyzed by GC-FID.

Spectroscopic Characterization. For IR analysis, self-supporting pellets (5 mm diameter, 6 mg) were pressed inside an Ar-filled glovebox. Spectra were also recorded inside the glovebox using a Bruker Alpha-FT-R spectrometer in the range 4000−400 cm^{-1}, accumulating 32 scans with 4 cm^{-1} resolution. Pyridine adsorption was performed in situ in an air-free Pyrex cell equipped with two IR-transparent KBr windows. A self-supporting pellet of $Cl-Al_2O_3$ (15 mg, 15 mm diameter) was pressed inside an Ar-filled glovebox and transferred into the in situ Pyrex cell. IR spectra were collected using a Shimadzu IRPrestige-21 spectrometer in the range 4000−400 cm^{-1} with 4 cm^{-1} resolution, accumulating 32 scans.

For solid-state NMR analysis, the highly air-sensitive samples were packed into 3.2 or 4 mm zirconia rotors inside an Ar-filled glovebox, and sealed with tightly fitting Kel-F caps. ^1H MAS NMR, $^1H-^1H$ DQ-SQ MAS NMR and $^1H-^{27}Al$ D-HMQC MAS NMR spectra were acquired on a Bruker Avance III 800 spectrometer (^1H, 800.13 MHz; ^{27}Al:, 208.50 MHz). For ^1H NMR experiments, the spinning frequency was 20 kHz, the optimized recycle delays were 1200 s ($Cl-Al_2O_3$) and 2 s (MTO−Cl-Al_2O_3), and 16 scans were collected using a 90° pulse excitation of 3.75 μs. ^{27}Al MAS NMR spectra at 18.8 T were acquired at a spinning frequency of 20 kHz in 3.2 mm rotors. D-HMQC experiments were set up with a ^{27}Al spin echo selective to the central transition, with pulses of 7.25 and 14.5 μs, and a ^1H $\pi/2$ pulse of 3 μs on either side of the ^{27}Al π pulse. A recycling delay of 2 s was used. The number of scans for each t_1 increment was set to 512. The $SR4^2_1$ dipolar recoupling scheme[119] was applied for 500 μs. Two-dimensional (2D) $^1H-^1H$ Double Quantum Magic-Angle Spinning experiments were performed at 20 kHz spinning speed using the $R12_2^5$ symmetry-based recoupling scheme,[120] applied for 116 μs at a radio frequency field strength of 40 kHz. A total of 16 transients were summed for each of the 300 t_1 increments, with a recycling delay of 2 s.

^{17}O MAS NMR spectra were recorded at 18.8 T (^{17}O: 108.5 MHz) in 3.2 mm rotors using either a single pulse or a central transition-

DOI: 10.1021/jacs.6b06953
J. Am. Chem. Soc. 2016, 138, 12935−12947

selective Hahn echo sequence, at a magic-angle spinning frequency of 20 kHz. Chemical shifts are reported in ppm with respect to TMS (tetramethylsilane), $Al(H_2O)_6^{3+}$, and H_2O as external references in ^1H, ^{27}Al, and ^{17}O NMR, respectively. ^{13}C NMR measurements were performed at room temperature on a Bruker AVANCE 300 NMR spectrometer operating at 75.4577 MHz with a spinning rate of 10 kHz. To enhance sensitivity in ^{13}C CP-MAS NMR experiments, isotopically labeled $^{13}CH_3ReO_3$ (>99% ^{13}C) was prepared according to a literature procedure.[81] ^{13}C CP-MAS spectra were recorded using a ^1H 90° pulse length of 3.5 μs, a contact time of 3 ms, an acquisition time of 21 ms, a recycle delay of 2 s, and high power proton decoupling during detection. ^1H and ^{13}C chemical shifts are referenced to *tetrakis*(trimethylsilyl)silane at 0.25 and 3.52 ppm, respectively.

X-ray absorption spectra at the Re L_I (12,527 eV) and L_{III} (10,535 eV) edges were collected at beamline 4−1 of the Stanford Synchrotron Radiation Lightsource, which operates at 3.0 GeV with a current of 500 mA. Samples were mounted in a He-filled cryostat at 15 K to minimize sample decomposition, and spectra were acquired in fluorescence mode using an Ar-filled Lytle detector. MTO was diluted (2 wt %) in BN (Sigma-Aldrich) to minimize self-absorption. Data were analyzed using the Demeter software package.[121] After subtraction of a linear pre-edge function, data were normalized by the edge height. A smooth, third-order polynomial approximating the absorption background of an isolated atom was subtracted to yield $\chi(k)$. The data were then k^3-weighted and Fourier-transformed. The number (N), distance (R), and mean-squared displacement (σ^2) of scattering atoms were assessed by nonlinear fitting with least-squares refinement in R-space using the EXAFS equation[122] as implemented in the Artemis software package.[121]

Catalytic Testing. Low pressure batch reactions were performed in a 120 mL tubular Pyrex reactor immersed in a water bath at 0 °C. Ten mg catalyst was transferred to the reactor in an Ar-filled glovebox. Propene (67 mbar, Praxair, 99.8%) was first purified by passage through dried molecular sieves (13X) and BTS catalyst (Sigma-Aldrich), then admitted into the evacuated reactor. Reaction products were analyzed by GC-FID (Shimadzu GC-2010) with separation on a capillary column (Supelco Alumina Sulfate plot, 30 m x 0.32 mm). The small amount of propane that is present as an impurity in the propene was used as the internal standard.

Flow reactions were carried out in a fixed-bed stainless steel reactor (1/4″ tube) operated in the up-flow configuration at 1 bar. The catalyst was loaded into the reactor in an Ar-filled glovebox and isolated using a 4-way valve, to allow extensive purging of the tube before passing the feed (pure propene) through the catalyst bed. The reactor was immersed in a constant temperature bath at 10 °C. The flow rate was controlled by a Brooks (5850S SMART) mass flow controller. To facilitate direct comparison of catalysts, the molar flow rate was held constant by adjusting the catalyst quantity and the propene flow rate. The products were analyzed by online GC (HP 6890), with separation by capillary column (50 m, KCl/Al_2O_3) and FID detection. Conversion and selectivity were calculated from the carbon balance obtained directly from the FID signals, according to eqs 1 and 2:

$$\text{conversion } \% = \frac{\text{mol propene converted}}{\text{mol propene introduced}} \times 100\% \quad (1)$$

$$\text{selectivity (for product } x) \% = \frac{\text{mol of product } (x)}{\text{mol propene converted}} \times 100\% \quad (2)$$

COMPUTATIONAL METHODS

All calculations began with a simple Al_2Cl_6 cluster model (Figure S15), containing both terminal and bridging Cl atoms. Three terminal chlorides of the cluster were fixed in space at optimal locations for the Al_2Cl_6 cluster. The fourth terminal chloride (Cl3) was allowed to move freely to enable its reaction with MTO. Bond angles and lengths are summarized in Tables S1 and S2. All calculations were performed with the ωB97X-D density functional[123] in Gaussian 09. The TZVP basis[124] was used for all light atoms, while the aug-def2-TZVP basis[125,126] as custom-optimized by Hwang et al.[127] was used for Re (aug-def2-TZVP is the def2-TZVP basis with a second f-orbital added, and with exponents of both f-primitives reoptimized to minimize the energy of perrhenate, ReO_4^-; it also uses an effective core potential to treat relativistic effects for Re).[128] A sample input file is included in the Supporting Information.

Computed free energies are reported at 298.15 K and include translational, rotational, and vibrational contributions for MTO. Models meant to represent surface species, including the Al_2Cl_6 cluster and its MTO adducts, include only vibrational contributions. The ^{13}C and ^1H NMR chemical shifts in Tables S3 and S4 were calculated using the GIAO method,[129,130] with calibration curves constructed from the computed shielding values and experimental chemical shifts of a series of well-known molecular Re compounds[131] (Figures S17, S18 and Tables S5, S6).

ASSOCIATED CONTENT

Supporting Information

The Supporting Information is available free of charge on the ACS Publications website at DOI: 10.1021/jacs.6b06953.

Sample calculations; additional IR, NMR, and XAS spectra and EXAFS curve fits; additional DFT-optimized structures and bond distances; NMR chemical shift calculations; coordinates and energies of all DFT-optimized structures (PDF)

AUTHOR INFORMATION

Corresponding Authors

*regis.gauvin@ensc-lille.fr
*mostafa.taoufik@univ-lyon1.fr
*baronp@engineering.ucsb.edu
*sscott@engineering.ucsb.edu

Notes

The authors declare no competing financial interest.

ACKNOWLEDGMENTS

Financial support of the U.S. Department of Energy, Office of Science, Division of Basic Energy Sciences, under the Catalysis Science Initiative (DE-FG-02-03ER15467) is gratefully acknowledged. J.R. is grateful for a Fulbright scholarship, and for the financial support by the Studienstiftung des Deutschen Volkes. We thank the CNRS, the French Ministry of Research and Higher Education, and the Agence Nationale de la Recherche (ANR-12-BS07-0021-01, OXOCAT) for their generous support. Financial support from the TGIR RMN THC Fr3050 is gratefully acknowledged. Portions of this work made use of the facilities of the Materials Research Laboratory (MRL) at UC Santa Barbara, supported by the NSF MRSEC Program under award DMR1121053. Use of the Stanford Synchrotron Radiation Lightsource, SLAC National Accelerator Laboratory, is supported by the U.S. Department of Energy, Office of Science, Office of Basic Energy Sciences, under Contract DE-AC02-76SF00515.

REFERENCES

(1) Mol, J. C. *J. Mol. Catal. A: Chem.* **2004**, *213*, 39.
(2) Balcar, H.; Cejka, J. *Coord. Chem. Rev.* **2013**, *257*, 3107.
(3) Lwin, S.; Wachs, I. E. *ACS Catal.* **2014**, *4*, 2505.
(4) Chaumont, P.; John, C. S. *J. Mol. Catal.* **1988**, *46*, 317.
(5) Cosyns, J.; Chodorge, J. A.; Commereuc, D.; Torck, B. *Hydrocarbon Process.* **1998**, *77*, 61.
(6) Duquette, L. G.; Cieslinski, R. C.; Jung, C. W.; Garrou, P. E. *J. Catal.* **1984**, *90*, 362.

DOI: 10.1021/jacs.6b06953
J. Am. Chem. Soc. 2016, 138, 12935−12947

(7) Xu, X.; Boelhouwer, C.; Vonk, D.; Benecke, J. I.; Mol, J. C. *J. Mol. Catal.* **1986**, *36*, 47.
(8) Boelhouwer, C. *J. Mol. Catal.* **1988**, *46*, 297.
(9) Schekler-Nahama, F.; Clause, O.; Commereuc, D.; Saussey, J. *Appl. Catal., A* **1998**, *167*, 237.
(10) Aguado, J.; Escola, J. M.; Castro, M. C.; Paredes, B. *Appl. Catal., A* **2005**, *284*, 47.
(11) Balcar, H.; Zilková, N.; Bastl, Z.; Dedecek, J.; Hamtil, R.; Brabec, L.; Zukal, A.; Cejka, J. *Stud. Surf. Sci. Catal.* **2007**, *170*, 1145.
(12) Balcar, H.; Hamtil, R.; Zilková, N.; Cejka, J. *Catal. Lett.* **2004**, *97*, 25.
(13) Balcar, H.; Hamtil, R.; Zilková, N.; Zhang, Z.; Pinnavaia, T. J.; Cejka, J. *Appl. Catal., A* **2007**, *320*, 56.
(14) Bakala, P. C.; Briot, E.; Millot, Y.; Piquemal, J.-Y.; Brégeault, J.-M. *J. Catal.* **2008**, *258*, 61.
(15) Jain, K. R.; Kühn, F. E. *J. Organomet. Chem.* **2007**, *692*, 5532.
(16) Herrmann, W. A.; Rost, A. M. J.; Mitterpleininger, J. K. M.; Szesni, N.; Sturm, S.; Fischer, R. W.; Kuehn, F. E. *Angew. Chem., Int. Ed.* **2007**, *46*, 7301.
(17) Tosh, E.; Mitterpleininger, J. K. M.; Rost, A. M. J.; Veljanovski, D.; Herrmann, W. A.; Kuehn, F. E. *Green Chem.* **2007**, *9*, 1296.
(18) Szesni, N.; Sturm, S.; Fischer, R.; Hermann, W. A. Improved process for preparing methyltrioxorhenium and organorhenium(VII) oxides. Patent WO 2009036775, March 26, 2009.
(19) Moses, A. W.; Leifeste, H. D.; Ramsahye, N. A.; Eckert, J.; Scott, S. L. *Chem. Ind. (Boca Raton, FL, U. S.)* **2007**, *115*, 13.
(20) Lai, Y.-Y.; Bornand, M.; Chen, P. *Organometallics* **2012**, *31*, 7558.
(21) Herrmann, W. A. *Angew. Chem., Int. Ed. Engl.* **1988**, *27*, 1297.
(22) Herrmann, W. A.; Wagner, W.; Flessner, U. N.; Volkhardt, U.; Komber, H. *Angew. Chem., Int. Ed. Engl.* **1991**, *30*, 1636.
(23) Rost, A. M. J.; Schneider, H.; Zoller, J. P.; Herrmann, W. A.; Kuehn, F. E. *J. Organomet. Chem.* **2005**, *690*, 4712.
(24) Moses, A. W.; Ramsahye, N. A.; Raab, C.; Leifeste, H. D.; Chattopadhyay, S.; Chmelka, B. F.; Eckert, J.; Scott, S. L. *Organometallics* **2006**, *25*, 2157.
(25) Moses, A. W.; Raab, C.; Nelson, R. C.; Leifeste, H. D.; Ramsahye, N. A.; Chattopadhyay, S.; Eckert, J.; Chmelka, B. F.; Scott, S. L. *J. Am. Chem. Soc.* **2007**, *129*, 8912.
(26) Stekrova, M.; Zdenkova, R.; Vesely, M.; Vyskocilova, E.; Cerveny, L. *Materials* **2014**, *7*, 2650.
(27) Buffon, R.; Auroux, A.; Lefebvre, F.; Leconte, M.; Choplin, A.; Basset, J. M.; Herrmann, W. A. *J. Mol. Catal.* **1992**, *76*, 287.
(28) Buffon, R.; Choplin, A.; Leconte, M.; Basset, J. M.; Touroude, R.; Herrmann, W. A. *J. Mol. Catal.* **1992**, *72*, L7.
(29) Bein, T.; Huber, C.; Moller, K.; Wu, C.-G.; Xu, L. *Chem. Mater.* **1997**, *9*, 2252.
(30) Salameh, A.; Baudouin, A.; Soulivong, D.; Boehm, V.; Roeper, M.; Basset, J.-M.; Copéret, C. *J. Catal.* **2008**, *253*, 180.
(31) Onaka, M.; Oikawa, T. *Chem. Lett.* **2002**, *31*, 850.
(32) Oikawa, T.; Ookoshi, T.; Tanaka, T.; Yamamoto, T.; Onaka, M. *Microporous Mesoporous Mater.* **2004**, *74*, 93.
(33) Oikawa, T.; Masui, Y.; Tanaka, T.; Chujo, Y.; Onaka, M. *J. Organomet. Chem.* **2007**, *692*, 554.
(34) Kotov, S. V.; Finkel'shtein, E. S.; Chernykh, S. P.; Shabalina, T. N.; Tyshchenko, V. A.; Milovantseva, V. I. *Kinet. Catal.* **2006**, *47*, 460.
(35) Pillai, S. K.; Abidli, A.; Belkacemi, K. *Appl. Catal., A* **2014**, *479*, 121.
(36) Tian, Q.; Larock, R. *J. Am. Oil Chem. Soc.* **2002**, *79*, 479.
(37) Biermann, U.; Metzger, J. O.; Meier, M. A. R. *Macromol. Chem. Phys.* **2010**, *211*, 854.
(38) Tovar, T. M.; Stewart, S. M.; Scott, S. L. *Top. Catal.* **2012**, *55*, 530.
(39) Pillai, S. K.; Hamoudi, S.; Belkacemi, K. *Appl. Catal., A* **2013**, *455*, 155.
(40) Popoff, N.; Mazoyer, E.; Pelletier, J.; Gauvin, R. M.; Taoufik, M. *Chem. Soc. Rev.* **2013**, *42*, 9035.
(41) Schrock, R. R. *Chem. Rev.* **2002**, *102*, 145.
(42) Copéret, C. *New J. Chem.* **2004**, *28*, 1.
(43) Jones, C. W. *Top. Catal.* **2010**, *53*, 942.
(44) Hübner, S.; de Vries, J. G.; Farina, V. *Adv. Synth. Catal.* **2016**, *358*, 3.
(45) Brégeault, J.-M.; El Ali, B.; Martin, J.; Martin, C.; Derdar, F.; Bugli, G.; Delamar, M. *J. Mol. Catal.* **1988**, *46*, 37.
(46) Hietala, J.; Root, A.; Knuuttila, P. *J. Catal.* **1994**, *150*, 46.
(47) Ono, Y. *Catal. Today* **2003**, *81*, 3.
(48) Knözinger, H.; Ratnasamy, P. *Catal. Rev.: Sci. Eng.* **1978**, *17*, 31.
(49) Delgado, M.; Delbecq, F.; Santini, C. C.; Lefebvre, F.; Norsic, S.; Putaj, P.; Sautet, P.; Basset, J.-M. *J. Phys. Chem. C* **2012**, *116*, 834.
(50) Mazoyer, E.; Trébosc, J.; Baudouin, A.; Boyron, O.; Pelletier, J.; Basset, J.-M.; Vitorino, M. J.; Nicholas, C. P.; Gauvin, R. M.; Taoufik, M.; Delevoye, L. *Angew. Chem., Int. Ed.* **2010**, *49*, 9854.
(51) Chauvin, Y.; Commereuc, D. *J. Chem. Soc., Chem. Commun.* **1992**, 462.
(52) Salameh, A.; Joubert, J.; Baudouin, A.; Lukens, W.; Delbecq, F.; Sautet, P.; Basset, J. M.; Copéret, C. *Angew. Chem., Int. Ed.* **2007**, *46*, 3870.
(53) Guillaume, D.; Gautier, S.; Despujol, I.; Alario, F.; Beccat, P. *Catal. Lett.* **1997**, *43*, 213.
(54) Digne, M.; Raybaud, P.; Sautet, P.; Guillaume, D.; Toulhoat, H. *J. Am. Chem. Soc.* **2008**, *130*, 11030.
(55) Kytokivi, A.; Lindblad, M.; Root, A. *J. Chem. Soc., Faraday Trans.* **1995**, *91*, 941.
(56) Thomson, J.; Webb, G.; Winfield, J. M. *J. Mol. Catal.* **1991**, *67*, 117.
(57) Zhang, W.; Sun, M.; Prins, R. *J. Phys. Chem. B* **2002**, *106*, 11805.
(58) Peri, J. B. *J. Phys. Chem.* **1965**, *69*, 211.
(59) Digne, M.; Sautet, P.; Raybaud, P.; Euzen, P.; Toulhoat, H. *J. Catal.* **2002**, *211*, 1.
(60) Rohner, M. C.; Sharma, V. K.; Richarz, W. *Chem. Eng. Technol.* **1989**, *12*, 27.
(61) Taoufik, M.; Szeto, K. C.; Merle, N.; Del Rosal, I.; Maron, L.; Trébosc, J.; Tricot, G.; Gauvin, R. M.; Delevoye, L. *Chem. - Eur. J.* **2014**, *20*, 4038.
(62) Busca, G. *Catal. Today* **2014**, *226*, 2.
(63) Herrmann, W. A.; Kiprof, P.; Rypdal, K.; Tremmel, J.; Blom, R.; Alberto, R.; Behm, J.; Albach, R. W.; Bock, H.; Bahmann, S.; Mink, J.; Lichtenberger, D.; Gruhn, N. E. *J. Am. Chem. Soc.* **1991**, *113*, 6527.
(64) Tebbe, F. N.; Parshall, G. W.; Reddy, G. S. *J. Am. Chem. Soc.* **1978**, *100*, 3611.
(65) LaPointe, A. M.; Schrock, R. R. *Organometallics* **1995**, *14*, 1875.
(66) Vicente, B. C.; Nelson, R. C.; Moses, A. W.; Chattopadhyay, S.; Scott, S. L. *J. Phys. Chem. C* **2011**, *115*, 9012.
(67) Wischert, R.; Copéret, C.; Delbecq, F.; Sautet, P. *ChemCatChem* **2010**, *2*, 812.
(68) Edwards, P.; Wilkinson, G. *J. Chem. Soc., Dalton Trans.* **1984**, 2695.
(69) Simpson, R. D.; Bergman, R. G. *Organometallics* **1993**, *12*, 781.
(70) Bare, S. R.; Kelly, S. D.; Vila, F. D.; Boldingh, E.; Karapetrova, E.; Kas, J.; Mickelson, G. E.; Modica, F. S.; Yang, N.; Rehr, J. J. *J. Phys. Chem. C* **2011**, *115*, 5740.
(71) Tougerti, A.; Cristol, S.; Berrier, E.; Briois, V.; La Fontaine, C.; Villain, F.; Joly, Y. *Phys. Rev. B: Condens. Matter Mater. Phys.* **2012**, *85*, 125136.
(72) Fröba, M.; Lochte, K.; Metz, W. *J. Phys. Chem. Solids* **1996**, *57*, 635.
(73) Malek, A.; Ozin, G. *Adv. Mater.* **1995**, *7*, 160.
(74) Herrmann, W. A.; Wojtczak, W. A.; Artus, G. R. J.; Kühn, F. E.; Mattner, M. R. *Inorg. Chem.* **1997**, *36*, 465.
(75) Noh, W.; Girolami, G. S. *Dalton Trans.* **2007**, 674.
(76) Edwards, A. J. *J. Chem. Soc., Dalton Trans.* **1972**, 582.
(77) Herrmann, W. A.; Kuchler, J. G.; Kiprof, P.; Riede, J. *J. Organomet. Chem.* **1990**, *395*, 55.
(78) West, N. M.; Labinger, J. A.; Bercaw, J. E. *Organometallics* **2011**, *30*, 2690.
(79) Weinstock, I. A.; Schrock, R. R.; Davis, W. M. *J. Am. Chem. Soc.* **1991**, *113*, 135.
(80) Bagnall, K. W.; Brown, D.; Colton, R. *J. Chem. Soc.* **1964**, 3017.

DOI: 10.1021/jacs.6b06953
J. Am. Chem. Soc. 2016, 138, 12935−12947

(81) Herrmann, W. A.; Kuchler, J. G.; Weischselbaumer, G.; Herdtweck, E.; Kiprof, P. *J. Organomet. Chem.* **1989**, *372*, 351.
(82) Herrmann, W. A.; Roesky, P. W.; Scherer, W.; Kleine, M. *Organometallics* **1994**, *13*, 4536.
(83) Herrmann, W. A.; Kuchler, J.; Felixberger, J. K.; Herdtweck, E.; Wagner, W. *Angew. Chem., Int. Ed. Engl.* **1988**, *27*, 394.
(84) Kress, J.; Wesolek, M.; Le Ny, J. P.; Osborn, J. A. *J. Chem. Soc., Chem. Commun.* **1981**, *0*, 1039.
(85) Kress, J.; Wesolek, M.; Osborn, J. A. *J. Chem. Soc., Chem. Commun.* **1982**, 514.
(86) Romão, C. C.; Kühn, F. E.; Herrmann, W. A. *Chem. Rev.* **1997**, *97*, 3197.
(87) Merle, N.; Girard, G.; Popoff, N.; De Mallmann, A.; Trébosc, J.; Berrier, E.; Paul, J.-F.; Del Rosal, I.; Maron, L.; Gauvin, R. M.; Delevoye, L.; Taoufik, M. *Inorg. Chem.* **2013**, *52*, 10119−10130.
(88) Kapteijn, F.; Homburg, E.; Mol, J. C. *J. Chem. Thermodyn.* **1983**, *15*, 147.
(89) Valla, M.; Wischert, R.; Comas-Vives, A.; Conley, M. P.; Verel, R.; Copéret, C.; Sautet, P. *J. Am. Chem. Soc.* **2016**, *138*, 6774.
(90) Leconte, M.; Basset, J.-M. *J. Am. Chem. Soc.* **1979**, *101*, 7296.
(91) Szeto, K. C.; Mazoyer, E.; Merle, N.; Norsic, S.; Basset, J.-M.; Nicholas, C. P.; Taoufik, M. *ACS Catal.* **2013**, *3*, 2162.
(92) Bilhou, J. L.; Basset, J. M.; Mutin, R.; Graydon, W. F. *J. Chem. Soc., Chem. Commun.* **1976**, 970.
(93) Flook, M. M.; Jiang, A. J.; Schrock, R. R.; Mueller, P.; Hoveyda, A. H. *J. Am. Chem. Soc.* **2009**, *131*, 7962.
(94) Jiang, A. J.; Zhao, Y.; Schrock, R. R.; Hoveyda, A. H. *J. Am. Chem. Soc.* **2009**, *131*, 16630.
(95) Marinescu, S. C.; Schrock, R. R.; Mueller, P.; Hoveyda, A. H. *J. Am. Chem. Soc.* **2009**, *131*, 10840.
(96) Marinescu, S. C.; Levine, D. S.; Zhao, Y.; Schrock, R. R.; Hoveyda, A. H. *J. Am. Chem. Soc.* **2011**, *133*, 11512.
(97) Townsend, E. M.; Schrock, R. R.; Hoveyda, A. H. *J. Am. Chem. Soc.* **2012**, *134*, 11334.
(98) Wang, C.; Haeffner, F.; Schrock, R. R.; Hoveyda, A. H. *Angew. Chem., Int. Ed.* **2013**, *52*, 1939.
(99) Bouhoute, Y.; Garron, A.; Grekov, D.; Merle, N.; Szeto, K. C.; De Mallmann, A.; Del Rosal, I.; Maron, L.; Girard, G.; Gauvin, R. M.; Delevoye, L.; Taoufik, M. *ACS Catal.* **2014**, *4*, 4232.
(100) Popoff, N.; Szeto, K. C.; Merle, N.; Espinas, J.; Pelletier, J.; Lefebvre, F.; Thivolle-Cazat, J.; Delevoye, L.; De Mallmann, A.; Gauvin, R. M.; Taoufik, M. *Catal. Today* **2014**, *235*, 41.
(101) Digne, M.; Sautet, P.; Raybaud, P.; Euzen, P.; Toulhoat, H. *J. Catal.* **2004**, *226*, 54.
(102) Pinto, H. P.; Nieminen, R. M.; Elliott, S. D. *Phys. Rev. B: Condens. Matter Mater. Phys.* **2004**, *70*, 125402.
(103) Bermudez, V. M. *J. Phys. Chem. C* **2009**, *113*, 1917.
(104) Rahane, A. B.; Deshpande, M. D.; Kumar, V. *J. Phys. Chem. C* **2011**, *115*, 18111.
(105) Fang, Z.; Wang, Y.; Dixon, D. *J. Phys. Chem. C* **2015**, *119*, 23413.
(106) Kovarik, L.; Genc, A.; Wang, C.; Qiu, A.; Peden, C. H. F.; Szanyi, J.; Kwak, J. H. *J. Phys. Chem. C* **2013**, *117*, 179.
(107) Rozita, Y.; Brydson, R.; Comyn, T. P.; Scott, A. J.; Hammond, C.; Brown, A.; Chauruka, S.; Hassanpour, A.; Young, N. P.; Kirkland, A. I.; Sawada, H.; Smith, R. I. *ChemCatChem* **2013**, *5*, 2695.
(108) Wischert, R.; Florian, P.; Copéret, C.; Massiot, D.; Sautet, P. *J. Phys. Chem. C* **2014**, *118*, 15292.
(109) Morris, L. J.; Downs, A. J.; Greene, T. M.; McGrady, G. S.; Herrmann, W. A.; Sirsch, P.; Scherer, W.; Gropen, O. *Organometallics* **2001**, *20*, 2344.
(110) Haw, J. F.; Richardson, B. R.; Oshiro, I. S.; Lazo, N. D.; Speed, J. A. *J. Am. Chem. Soc.* **1989**, *111*, 2052.
(111) Chen, E. Y.-X.; Marks, T. J. *Chem. Rev.* **2000**, *100*, 1391.
(112) Youinou, M. T.; Kress, J.; Fischer, R.; Aguero, A.; Osborn, J. A. *J. Am. Chem. Soc.* **1988**, *110*, 1488.
(113) Schofield, M. H.; Schrock, R. R.; Park, L. Y. *Organometallics* **1991**, *10*, 1844.
(114) Blosch, L. L.; Abboud, K.; Boncella, J. M. *J. Am. Chem. Soc.* **1991**, *113*, 7066.
(115) Flatt, B. T.; Grubbs, R. H.; Blanski, R. L.; Calabrese, J. C.; Feldman, J. *Organometallics* **1994**, *13*, 2728.
(116) Peryshkov, D. V.; Schrock, R. R.; Takase, M. K.; Müller, P.; Hoveyda, A. H. *J. Am. Chem. Soc.* **2011**, *133*, 20754.
(117) McDaniel, M. P.; Jensen, M. D.; Jayaratne, K.; Collins, K. S.; Benham, E. A.; McDaniel, N. D.; Das, P. K.; Martin, J. L.; Yang, Q.; Thorn, M. G.; Masino, A. P. In *Tailor-Made Polymers: Via Immobilization of Alpha-Olefin Polymerization Catalysts*; Severn, J. R., Chadwick, J. C., Eds.; Wiley-VCH: Weinheim, 2008; pp 171−210.
(118) Prades, F.; Broyer, J.-P.; Belaid, I.; Boyron, O.; Miserque, O.; Spitz, R.; Boisson, C. *ACS Catal.* **2013**, *3*, 2288.
(119) Brinkmann, A.; Kentgens, A. P. M. *J. Am. Chem. Soc.* **2006**, *128*, 14758.
(120) Carravetta, M.; Eden, M.; Zhao, X.; Brinkmann, A.; Levitt, M. H. *Chem. Phys. Lett.* **2000**, *321*, 205.
(121) Ravel, B.; Newville, M. *J. Synchrotron Radiat.* **2005**, *12*, 537.
(122) Sayers, D. E.; Stern, E. A.; Lytle, F. *Phys. Rev. Lett.* **1971**, *27*, 1204.
(123) Chai, J.-D.; Head-Gordon, M. *Phys. Chem. Chem. Phys.* **2008**, *10*, 6615.
(124) Schäfer, A.; Huber, C.; Ahlrichs, R. *J. Chem. Phys.* **1994**, *100*, 5829.
(125) Weigend, F.; Ahlrichs, R. *Phys. Chem. Chem. Phys.* **2005**, *7*, 3297.
(126) Feller, D. *J. Comput. Chem.* **1996**, *17*, 1571.
(127) Hwang, T.; Goldsmith, B. R.; Peters, B.; Scott, S. L. *Inorg. Chem.* **2013**, *52*, 13904.
(128) Andrae, D.; Häußermann, U.; Dolg, M.; Stoll, H.; Preuß, H. *Theoret. Chim. Acta* **1990**, *77*, 123.
(129) Forsyth, D. A.; Sebag, A. B. *J. Am. Chem. Soc.* **1997**, *119*, 9483.
(130) White, R. E.; Hanusa, T. P. *Organometallics* **2006**, *25*, 5621.
(131) Cai, S.; Hoffman, D. M.; Wierda, D. A. *Organometallics* **1996**, *15*, 1023.

DOI: 10.1021/jacs.6b06953
J. Am. Chem. Soc. 2016, 138, 12935−12947